Chinese Chemical Letters 37 (2026) 111580

Contents lists available at ScienceDirect

Chinese Chemical Letters

journal homepage: www.elsevier.com/locate/cclet

# Hypertaxoids A and B, two unique meroterpenoids from *Hypericum elatoides* as microtubule stabilizers and their antiproliferative effects on cervical cancer

Jin-Yan Xie[a,1], Yu-Qi Gao[b,1], Wu-Yang Liu[a], Sheng-Yong Zhang[a], Ding Li[a], Wen-Ji Wang[a], Jiang-Jiang Tang[a,*], Jin-Ming Gao[a,*]

[a] Shaanxi Key Laboratory of Natural Products and Chemical Biology, College of Chemistry and Pharmacy, Northwest A&F University, Yangling 712100, China
[b] College of Food Science and Technology, Northwest University, Xi'an 710069, China

ARTICLE INFO

*Article history:*
Received 22 April 2025
Revised 8 July 2025
Accepted 10 July 2025
Available online 10 July 2025

*Keywords:*
Hypericum elatoides
Polycyclic polyprenylated acylphloroglucinols meroterpenoids
Structure elucidation
Anti-cervical cancer
Tubulin polymerization promotors

ABSTRACT

Hypertaxoids A (Hyp A, **1**) and B (Hyp B, **2**), two highly modified benzoyl polycyclic polyprenylated acylphloroglucinols (PPAPs) with an unprecedented carbon skeleton, were isolated from the aerial parts of Hypericum elatoides. Compounds **1** and **2** share a bicyclo[5.3.1]hendecane motif fused a 1,1-dimethylcyclohexane unit, with a taxoid-like 6/8/6 tricyclic core, while compound **1** possesses a new 6/8/6/5 tetracyclic ring system. Their structures were elucidated by a combination of nuclear magnetic resonance spectroscopy (NMR) analysis, high resolution electrospray ionization mass spectroscopy (HRESIMS), X-ray crystallography, and electronic circular dichroism (ECD) calculations. A key cation-anion progress in formation mechanism of **1** and **2** was revealed based on density functional theory (DFT) calculations. Among them, hypertaxoid B displayed selective inhibition on cell growth of human cervical cancer lines. The mechanism of action revealed that Hyp B could stabilize tubulin polymerization and disrupt the microtubule network, leading to apoptosis in C-33A cells through the mitochondria signaling pathway. Moreover, Hyp B significantly suppressed the C-33A tumor growth, brain metastasis, and angiogenesis in zebrafish xenograft models. Compound **2** represents the first tubulin polymerization-promoting natural product of PPAPs, which highlights it as a promising lead compound with a new type of skeleton for antineoplastic drug development for cervical cancer treatment.

© 2026 Published by Elsevier B.V. on behalf of Chinese Chemical Society and Institute of Materia Medica, Chinese Academy of Medical Sciences.

Cervical cancer is the second most common malignancy, with around 570,000 new cases and 311,000 deaths every year, among women worldwide. The incidence and mortality of cervical cancer in low- and middle-income countries are second only to breast cancer [1]. China has approximately 130,000 new cases from cervical cancer annually, accounting for 28 % of the total cervical cancer cases globally [2]. Currently, a combination of cisplatin-based chemotherapy with radiation is the most effective treatment for cervical cancer [3]. However, the clinical use of this combination treatment is restricted due to severe side effects, such as neurotoxicity, nephrotoxicity, and chemoresistance [4]. Consequently, it is imperative to exert significant endeavors in the quest for a new effective and targeted agent for treating the cancer with diminished toxicological implications [5].

The genus *Hypericum* is one of the largest genera of the family Hypericaceae, comprising more than 500 species throughout the world [6], and some of the species have been historically used as ethnomedicines or folk medicines for treatment diseases [7,8]. Plants of the *Hypericum* genus are well-known for a group of special bioactive meroterpenoids, polycyclic polyprenylated acylphloroglucinols (PPAPs), which are biogenetically derived from acylphloroglucinol cores densely decorated with prenyl, geranyl, or more highly substituted side-chain substituents. PPAPs are a fascinating family of natural products, most of which feature a bicyclo[3.3.1]nonane-2,4,9-trione (bicyclic polyprenylated acylphloroglucinols, BPAPs), tricyclo[3.3.1.1]decane (adamantane), tricyclo[4.3.1.1]undecane (homoadamantane), octahydrospiro[cyclohexan-1,5′indene]−2,4,6-trione (spirocyclic PPAPs) frameworks and other type of PPAPs. To date, there are a multitude of structural diversity of PPAPs mainly isolated from the *Hypericum* genus [9–12], which exhibit remarkably broad range of biological activities including anti-inflammatory [13], cytotoxic [14], antidepressant [15], antimicrobial [16], antioxidant

* Corresponding authors.
*E-mail addresses:* tangjiang11@nwsuaf.edu.cn (J.-J. Tang), jinminggao@nwsuaf.edu.cn (J.-M. Gao).
[1] These authors contributed equally to this work.

https://doi.org/10.1016/j.cclet.2025.111580
1001-8417/© 2026 Published by Elsevier B.V. on behalf of Chinese Chemical Society and Institute of Materia Medica, Chinese Academy of Medical Sciences.

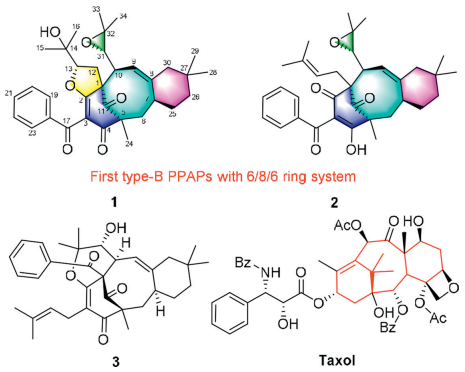



**Fig. 1.** Structures of **1**–**3** and taxol.

[17], and anti-neurodegenerative [18,19] activities. Among the structural diversity of PPAPs, there has been limited reporting on 6/8/6 scaffold PPAPs featuring a bicyclo[5.3.1]hendecane core, with most being type-A and no literature reports on type-B PPAPs of 6/8/6 ring system (Fig. S1 in Supporting information). And recent investigations revealed that some type-B PPAPs have antineoplastic potential, such as oblongifolin C [20].

*Hypericum elatoides* (*H. elatoides*) is a perennial herb grown as a narrow endemic species in the Qinling areas of Shaanxi province in northwestern China. As part of our ongoing works to study the chemical diversity of *Hypericum* species and their biological activities [21–27], two PPAPs with a new carbon skeleton, hypertaxoids A and B (**1** and **2**) (Fig. 1), along with a known analog, hyperprin B (**3**) (Fig. 1) [28], were isolated from the aerial parts of *H. elatoides*. To the best of our knowledge, compounds **1** and **2** were characterized to be a type-B [5.3.1]-core PPAPs, of which **2** possesses a 6/8/6 tricyclic system, and **1** featured a 5/6/8/6 tetracyclic skeleton. Notably, this is the first report on type-B PPAPs, which linked a benzoyl at C-3, sharing a common taxoid-like 6/8/6 tricyclic architecture with bicyclo[5.3.1]hendecane core, representing a new category of PPAPs in natural products. Their structures, including absolute configurations, were determined by spectroscopic data, X-ray crystallography, and electronic circular dichroism (ECD) calculations. Subsequently, inspiration by the similar 6/8/6 carbon skeleton of **1** and **2** with anticancer taxane-type compounds, such as taxol, encouraged us to perform anticancer evaluations of these compounds, and **2** showed selective cytostatic activity against human cervical cancer cells (C-33A). Furthermore, the mechanism of action experiments revealed that **2** may associate with tubulin, promote tubulin polymerization, and disrupt mitotic spindle integrity to display its inhibition effects of proliferation, migration, brain metastasis and angiogenesis. These results above all demonstrated that **2**, with a taxoid-like carbon skeleton, is the first PPAP that acts as a tubulin polymerization stabilizer and may be a potential lead compound in anticancer drug development.

Hypertaxoid A (**1**) had the molecular formula $C_{34}H_{42}O_6$ based on the positive high resolution electrospray ionization mass spectroscopy (HRESIMS) (*m/z* 547.3063 $[M+H]^+$, calcd. for $C_{34}H_{43}O_6$, 547.3060). The infrared radiation (IR) spectrum showed obvious absorption bands for hydroxyl (3448 $cm^{-1}$), and carbonyl (1713 and 1643 $cm^{-1}$), respectively. The $^1H$ nuclear magnetic resonance spectroscopy (NMR) spectrum along with the heteronuclear single quantum coherence (HSQC) spectrum, exhibited the presence of an unusual monosubstituted benzene moiety with five protons [$\delta_H$ 7.79 (d, $J=7.7$ Hz, 2H), 7.56 (t, $J=7.7$ Hz, 1H), and 7.45 (t, $J=7.7$ Hz, 2H)], one trisubstituted olefin [$\delta_H$ 4.89 (d, $J=8.0$ Hz, 1H)], four methines [$\delta_H$ 4.69 (dd, $J=9.3$, 6.7 Hz, 1H), 2.79 (d, $J=9.4$ Hz, 1H), 2.51, and 2.19], five methylenes [$\delta_H$ 2.86 (1H, dd, 13.5, 6.7)/2.52, 2.53/1.44, 1.66/1.39, and 1.44/1.21], and seven methyl singlets [$\delta_H$ 1.35, 1.29, 1.20, 1.18, 1.13, 0.95, 0.75] (Table S1 in Supporting information). The $^{13}C$ NMR and distortionless enhancement by polarization transfer (DEPT) spectra showed 34 carbon signals corresponding to one phenyl group, three carbonyl groups, four double carbons, five quaternary carbons, four methine carbons, five methylene carbons and seven methyl carbons. These analyses suggested that **1** was a PPAP derivative. The $^1H$–$^1H$ correlation spectroscopy (COSY) spectrum which showed two spin systems, H-6b/H-7, and H-9/H-10 as depicted by blue bonds (Fig. 2A), and heteronuclear multiple bond correlation (HMBC) correlations of $H_3$–24 to C-4, C-5, C-6 and C-11, H-6a to C-4 and C-8, H-10 to C-2 and C-8, and H-7 to C-5 and C-8 constructed the bicyclo[5.3.1]hendecane core [12] in compound **1**. And a 1,1-dimethylcyclohexane unit was defined by the HMBC correlations of $H_2$–30 to C-8, C-9, C-27 and $H_3$–28/$H_3$–29 to C-26, C-27, C-30, along with the H-6b/H-7/H-25a/H-26b spin system [28]. The locations of the monosubstituted benzene ring at C-17 was elucidated by HMBC correlations of H-19/23 to C-17. The remaining resonances were identified as a 2-(2–hydroxy-dimethylmethane)-furan ring at C-1–C-2 and 2,2-dimethyl-epoxypropane moiety at C-10 by strong HMBC correlations from $H_3$–15/$H_3$–16 to C-13, C-14, C-15 and C-16, from $H_2$–12 to C-2, C-10 and C-14, from $H_3$–33 and $H_3$–34 to C-31, C-32, C-33 and C-34, and from H-10 to C-1, C-2, C-9, and C-31, with the COSY cross-peaks of $H_2$–12/H-13 and H-9/H-10/H-31. The planar structure of **1** was therefore furnished as depicted.

The relative configurations of compound **1** was elucidated by analysis of the nuclear overhauser effect spectroscopy (NOESY) spectrum. The H-12b/H-10, H-10/H-7, H-7/H-6a, and H-6a/$H_3$–24 NOESY correlations (Fig. 2A) implied their co-facial relationship, suggesting H-7, H-10 and Me-24 were $\alpha$-orientation. The large coupling constant of H-10/H-31 ($J=9.4$ Hz) and the H-31/H-13 NOESY correlation indicated the axially *trans*-oriented H-10 and H-31, and H-13 was $\beta$-oriented. The absolute configurations of **1** was determined by a comparison of the experimental ECD data with the calculated ECD data (Fig. 2B). The results revealed that the absolute configuration of **1** was determined to be 1*R*,5*R*,7*S*,10*S*,13*S*,31*S*. To further validate the absolute configuration of **1**, a high-quality crystal of **1** was obtained in a mixed solvent ($CH_2Cl_2$/$H_2O$, 2:1), which facilitated an X-ray crystallographic measurement *via* Cu K$\alpha$ radiation [Flack parameter = 0.01 (17), CCDC 2225882] (Fig. 2C). Thus, its structure, named hypertaxoid A, was determined as shown.

Hypertaxoid B (**2**) was isolated as a colorless oil. Its molecular formula was established to be $C_{34}H_{42}O_5$ from its $^{13}C$ NMR and HRESIMS data (*m/z* 553.2919 $[M+Na]^+$, calcd. for $C_{34}H_{42}NaO_5$, 553.2930), corresponding to 14 degrees of unsaturation. The IR spectrum showed absorption bands of hydroxyl (3435 $cm^{-1}$), and carbonyl (1738 and 1700 $cm^{-1}$) groups. The $^1H$ NMR spectrum of **2** showed signals indicative of five aromatic protons at $\delta_H$ 7.52 (d, $J=7.4$ Hz, 2H), 7.50 (t, $J=7.4$ Hz, 1H), and 7.40 (t, $J=7.4$ Hz, 2H), two olefinic protons at $\delta_H$ 4.78 (t, $J=6.9$ Hz, 1H) and 4.75 (dd, $J=8.7$, 1.7 Hz, 1H), an oxygenated methine proton at $\delta_H$ 3.30 (d, $J=8.7$ Hz, 1H), and seven methyl singlets [$\delta_H$ 1.72, 1.62, 1.41, 1.34, 1.12, 0.83, 0.65]. The $^{13}C$ NMR, DEPT and HSQC data showed 34 carbon signals, including an enolic $\beta$-diketone system (C-2, C-3, and C-4), two ketone carbonyls, four olefinic carbons, six aromatic carbons, four quaternary carbons, three methine carbons, five methylene carbons, and seven methyl carbons. Extensive analyses of the 1D and 2D NMR data of **2** implied that **2** possesses a similar structure to **1** (Fig. 1). A further comparison of the NMR data of **2** with those of **1** indicated that **2** also had a 6/8/6-fused core and had the same substitution at C-10 as those in **1**. The HMBC correlations from $H_2$–12 to C-1, C-2 and C-10 and from H-13 to C-14, C-15 and C-16, and $^1H$–$^1H$ COSY correlations of H-13/$H_2$–12 suggested a prenylated group at C-1. One carbonyl group ($\delta_C$ 192.2) was assigned at C-2, on the basis of the HMBC correlations from $H_2$–12 to C-2 and from H-10 to C-2. Therefore, the planar structure

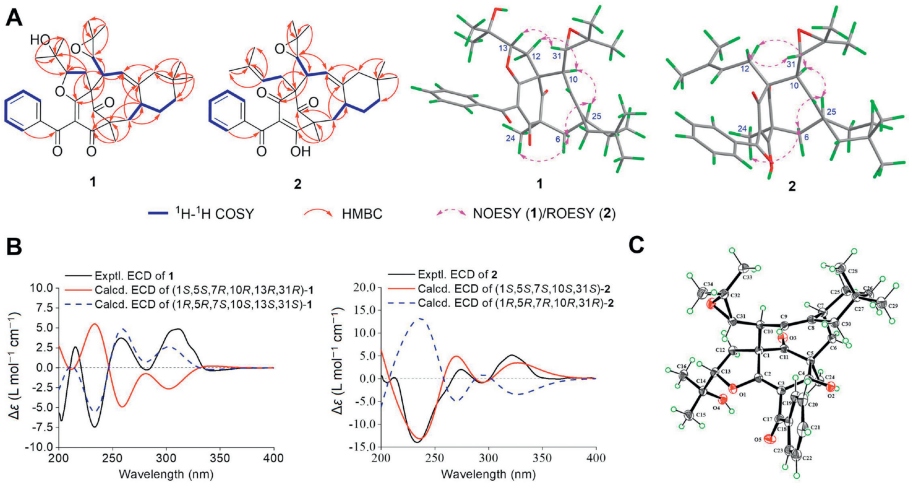
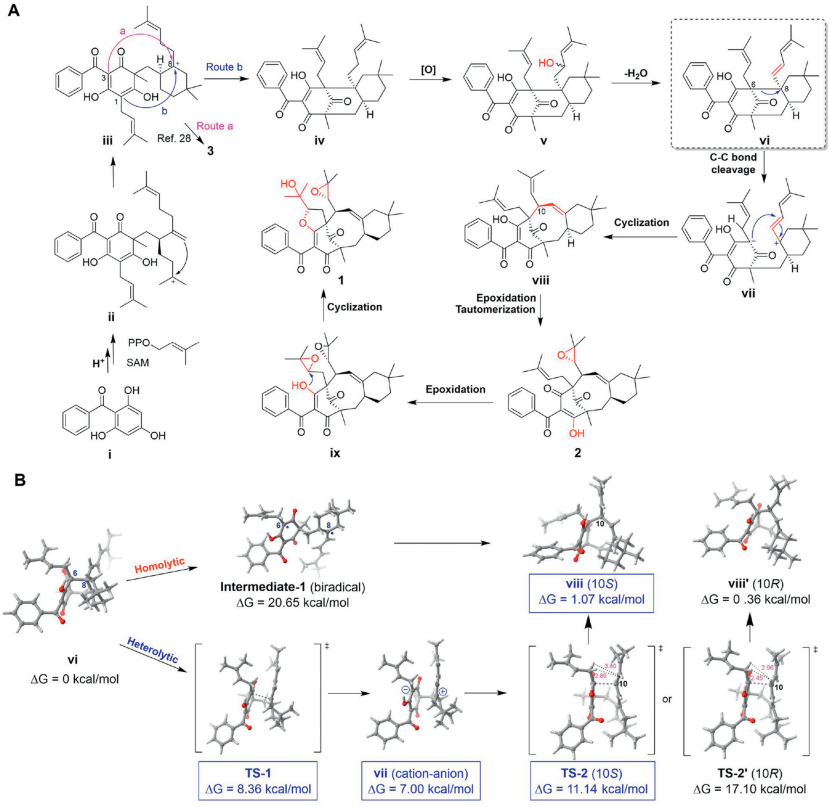



**Fig. 2.** (A) Key $^1$H–$^1$H COSY (blue), HMBC (red arrows), and NOESY/ROESY (double-headed arrows) correlations of **1** and **2**. (B) Experimental and calculated ECD spectra of **1** and **2**. (C) X-ray crystal structure of **1** (CCDC: 2225882).




**Scheme 1.** (A) The plausible formation mechanism of **1** and **2**. (B) DFT-calculated energies profiles for possible reactions from **vi** to **viii** *via* homolytic (intermediate-1 of free radical progress) and heterolytic (TS-1, **vii**, and TS-2 of cation-anion progress).

of **2** closely resembled that of **1**, with the only difference being that **2** possesses an isopentenyl group at C-1 and a carbonyl group at C-2 instead of a tetrafuran ring which was formed by the C-1 isoprenyl-derived unit and the C-2 carbonyl group in **1**.

The ROESY correlations of H-12a/H-10, H-10/H-7, H-7/H-6a, and H-6a/H$_3$–24 showed that H-7, H-10, and Me-24 were co-facial and assigned as $\alpha$-oriented (Fig. 2A), while the configuration of C-31 was confirmed as $\beta$-oriented by the cross-peaks of the large coupling constant of H-10/H-31 ($J$ = 8.7 Hz) and H-12b/H-31. Combining biogenetic pathway, the relative configuration of **2** was assigned as 1*S**,5*S**,7*S**,10*S**,31*S**. Subsequently, the absolute configuration of **2** was determined by comparing its experimental and calculated ECD spectra, and the calculated ECD spectrum of (1*S*,5*S*,7*S*,10*S*,31*S*)-**2** was in good agreement with the experimental ECD spectrum (Fig. 2B). Finally, the absolute configuration of **2** was unambiguously assigned as 1*S*,5*S*,7*S*,10*S*,31*S*, named hypertaxoid B.

Hypertaxoids A (**1**) and B (**2**) represent the first examples of a new category of naturally-occurring type-B PPAPs with a 6/8/6 ring core linked a benzoyl group at C-3, and a plausible biogenetic pathway for **1** and **2** were proposed in Scheme 1A with 2,4,6-trihydroxybenzophenone (**i**) as the precursor **i** would be converted to intermediate **ii** *via* a cascade of alkylations, accompanied by intramolecular cyclization to give a key carbocation intermediate **iii**, from which compound **3** could be generate by the attack from C-3 to C-8 (route a) [28]. The another attack mode which from C-1 to C-8 (route b) builds the type-B PPAP skele-

ton with bicyclo[3.3.1]nonane core in intermediate **iv**. By oxidation and dehydration, **iv** would give intermediates **v** and **vi**, respectively. After heterolytic cleavage, intermediate **iv** would give a cation-anion intermediate **vii**, which further submits cyclization to give intermediate **viii** with bicyclo[5.3.1]hendecane scaffold. Subsequent cyclization, epoxidation, and tautomerization in **viii** could give rise to **1** and **2**. Notably, the process from intermediate **vi** to **viii** has been proposed to occur with a homolytic cleavage at single bond of C-6 and C-8 and subsequent radical-radical combination in one biosynthetic congener, hyperprin B (**3**) [28]. In order to explore the plausible formation of **viii**, a computational study was then carried out to investigate the mechanistic key details of the free radical progress and cation-anion progress (Scheme 1B). The DFT calculations showed that the homolytic cleavage has intermediate-1 at high energy of 20.65 kcal/mol, suggesting that this free radical process is infeasible in thermodynamics. The heterolytic cleavage of **iv** has a lower transition state TS-1 (8.36 kcal/mol), intermediate **vii** (7.00 kcal/mol), and a relatively low transition state TS-2 (11.14 kcal/mol) to form **viii**, indicating that this cation-anion progress is favorable in kinetics and thermodynamics. The stereoisomer (10*R*)-**viii'** (0.36 kcal/mol) is thermodynamically more favorable than (10*S*)-**viii** (1.07 kcal/mol), but due to the influence of steric hindrance, the activation barrier of the transition state (10*S*)-TS-2 is about 6 kcal/mol lower than that of (10*R*)-TS-2′ (17.10 kcal/mol), resulting in the rapid formation of the desired products. Therefore, combining the DFT calculations, it is speculated that a cation-anion progress is involved in the formation of **1** and **2**.

Due to the potent cytotoxic activities reported for several benzoyl-PPAPs and the taxoid-like characteristics of **1** and **2** with a benzoyl group featuring a 6/8/6 tricyclic skeleton, these compounds were initially assessed for their cytotoxic activity against six human solid tumor cell lines LNCaP, LECP$\alpha-1$, MKN-45, MDA-MB-468, A2780 and C-33A. As shown in Fig. 3A and Table S2 (Supporting information), the cervical cancer cell line C-33A showed strong sensitivity to Hyp B with half maximal inhibitory concentration ($IC_{50}$) value of 7.4 μmol/L, and had no cytotoxic effect ($IC_{50}$ > 50 μmol/L, more than 95% cell viability at 20 μmol/L) on the two normal cell lines HCerEpic (cervical epithelial) and 293T (embryonic kidney). In addition, Hyp B significantly inhibited the colony formation of C-33A cells at 5 and 10 μmol/L compared to the control group (Figs. 3B and C). In order to determine the efficacy of Hyp B on the proliferation of cancer cells *in vivo*, an antineoplastic experiment was performed on C-33A cells in a zebrafish xenograft model (Fig. 3D), which is a popular vertebrate model for biomedical research [29]. The results demonstrated that the treatment effects observed in the groups treated with 1.25 and 2.5 μmol/L of Hyp B were comparable to that of the taxol group (5 μmol/L) (Figs. 3E–G). Furthermore, it was observed that Hyp B significantly increased the expression levels of c-caspase-3 and c-PARP, indicating that it can induce cell apoptosis by regulating the mitochondria-mediated caspase activation pathway (Figs. S3A–G in Supporting information). Based on antitumor mechanistic insights of taxol, we investigated the effect on microtubule stabilization. The findings suggest that Hyp B promote tubulin polymerization by binding to the toxin domain of $\beta$-tubulin, further inhibiting mitosis in C-33A cells and inducing the formation of abnormal spindles (Figs. S4A–G, S5A and B in Supporting information).

The process of cancer metastasis involves the spread of malignant tumor cells from the primary site to other locations through blood vessels, body cavities, or lymphatic pathways, leading to continued proliferation [30]. This phenomenon is a major contributing factor to the failure of most tumor treatments [31]. And microtubules play a crucial role in regulating cell growth and division, facilitating cell motility, maintaining cellular morphology, and controlling intracellular trafficking [32]. Following the results

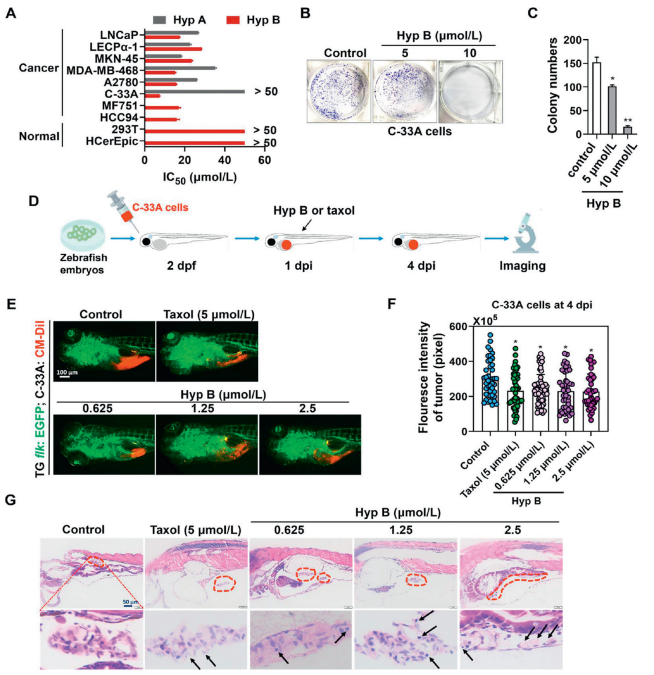



**Fig. 3.** Inhibitory effects of Hyp B on cancer cells proliferation *in vitro* and *in vivo*. (A) The $IC_{50}$ values on the cell viabilities of eight human cancer cell lines for 48 h, $n = 3$. (B) Colony formation assay of C-33A cells treated with or without Hyp B for 2 weeks. (C) Quantitative analysis of colony formation, $n = 3$. (D) Experimental workflow of zebrafish treatments. (E) Proliferation of C-33A cells in the zebrafish xenografted model under treatment with or without Hyp B and taxol at 4 days post injection (dpi) (3 days post transplantation (dpt)). Scale bar: 100 μm. (F) Quantitative analysis of cell proliferations in the zebrafish xenografted model after treatment with or without Hyp B and taxol, $n \geq 40$. (G) Hematoxylin-eosin staining of zebrafish xenografted with C-33A cells at 4 dpi (3 dpt) with or without Hyp B and taxol. Scale bar: 50 μm. Arrows point to necrotic or apoptotic C-33A cells. Data were presented as mean ± SEM. $^{*}P < 0.05$, $^{**}P < 0.01$ *vs.* the control (DMSO) group.

of effect on tubulin polymerization analysis, we further verified the potent suppressive effect of Hyp B on C-33A cell migration. Our findings indicated that it could significantly inhibit C-33A cell migration, and the expressions of migration-related proteins MMP2, MMP9 and $\beta$-certain all showed a decreasing trend, which treated with Hyp B (Figs. S6A–D in Supporting information). Meanwhile, in our experiments it also significantly inhibited brain metastasis of cancer cells and tumor-induced angiogenesis in the zebrafish cervical cancer model (Figs. S6E, F and S8A, B in Supporting information), but no tail metastasis (Fig. S7 in Supporting information).

In conclusion, hypertaxoids A and B, the first examples of a type-B [5.3.1]-core fused a 1,1-dimethylcyclohexane unit PPAPs, similar with a 6/8/6 tricyclic scaffold of taxoid analogs, were isolated from *H. elatoides*. The mechanism of anticancer activity suggested that Hyp B may engage in interactions with tubulin, promote tubulin polymerization, and disrupt mitotic spindle integrity to manifest its inhibitory effects on the proliferation, migration, brain metastasis, and angiogenesis of C-33A cells both *in vivo* and *in vitro*, which represented the first tubulin polymerization-promoting natural product of PPAPs. Thus, Hyp B represents a novel microtubule-stabilizing agent that suppresses tubulin depolymerization through the toxin domain of $\beta$-tubulin binding, which provides a new template structure for further design of more promising candidate.

## Declaration of competing interest

The authors declare that they have no known competing financial interests or personal relationships that could have appeared to influence the work reported in this paper.

## CRediT authorship contribution statement

**Jin-Yan Xie:** Writing – original draft, Methodology, Investigation, Formal analysis. **Yu-Qi Gao:** Methodology, Formal analysis. **Wu-Yang Liu:** Methodology, Formal analysis. **Sheng-Yong Zhang:** Conceptualization. **Ding Li:** Formal analysis, Data curation. **Wen-Ji Wang:** Formal analysis, Data curation. **Jiang-Jiang Tang:** Writing – original draft, Formal analysis, Conceptualization. **Jin-Ming Gao:** Writing – review & editing, Supervision, Methodology, Investigation, Funding acquisition, Conceptualization.

## Acknowledgments

The work was financially supported by the National Natural Science Foundation of China (Nos. 32201249, 22277099), and QinChuangYuan Scientists+Engineers Team Construction Project (No. 2023KXJ-214). The authors would like to thank Life Science Research Core Service at Northwest A&F University (Luqi Li) for the HRESIMS data, and the State Key Laboratory of Fluorine & Nitrogen Chemicals (Minchang Wang), Xi'an Modern Chemistry Research Institute, for the 800 MHz NMR data.

## Supplementary materials

Supplementary material associated with this article can be found, in the online version, at doi:10.1016/j.cclet.2025.111580.

## References

[1] X. Yang, J. An, Y. Zhang, et al., Front. Oncol. 10 (2020) 591700.
[2] W.Y. Wang, Y.X. Cao, X. Zhou, et al., Drug Des. Devel. Ther. 13 (2019) 2205–2213.
[3] S. Ramakrishnan, S. Partricia, G. Mathan, Biomed. Pharmacother. 70 (2015) 103–110.
[4] P.G. Rose, B.N. Bundy, E.B. Watkins, et al., N. Engl. J. Med. 3 (1999) 1144–1153.
[5] M. Hawash, N. Jaradat, A.M. Eid, et al., BMC Chem. 16 (2022) 47.
[6] S.L. Crockett, N.K.B. Robson, Med. Aromat. Plant Sci. Biotechnol. 5 (2011) 1–13.
[7] G.I. Caldeira, L.P. Gouveia, R. Serrano, et al., Plants 11 (2022) 2509.
[8] M. Marrelli, G. Statti, F. Conforti, Mini. Rev. Med. Chem. 20 (2020) 66–87.
[9] N.N. Jiang, Y.S. Ye, X. Liu, et al., Org. Lett. 25 (2023) 8965–8969.
[10] C.M. Yuan, Y.R. Zeng, L. Huang, et al., Chin. Chem. Lett. 36 (2025) 109859.
[11] Z.Y. Shi, J. Yin, Y. Xiao, et al., Chin. Chem. Lett. 35 (2024) 109458.
[12] W.J. Xu, P.F. Tang, W.J. Lu, et al., Org. Lett. 21 (2019) 8558–8562.
[13] F.V. Santa-Cecília, L.A.S. Freitas, F.C. Vilela, et al., Eur. J. Pharmacol. 670 (2011) 280–285.
[14] H.C. Zhu, C.M. Chen, D.D. Tan, et al., RSC Adv. 6 (2016) 86710–86716.
[15] O. Grundmann, Y. Lv, O. Kelber, et al., Neuropharmacology 58 (2010) 767–773.
[16] A. Oya, N. Tanaka, T. Kusama, et al., J. Nat. Prod. 78 (2015) 258–264.
[17] L. Verotta, Phytochem. Rev. 1 (2002) 389–407.
[18] Y. Guo, N. Zhang, C.M. Chen, et al., J. Nat. Prod. 80 (2017) 1493–1504.
[19] J.A. Richard, R.H. Pouwer, D.Y.K. Chen, Angew. Chem. Int. Ed. 51 (2012) 4536–4561.
[20] X.W. Yang, R.B. Grossman, G. Xu, Chem. Rev. 118 (2018) 3508–3558.
[21] W.Y. Liu, X.X. Lei, W.J. Wang, et al., Chin. Chem. Lett. 36 (2025) 110478.
[22] W.Y. Liu, L.L. Gao, W. Zhou, et al., Phytochemistry 235 (2025) 114450.
[23] W.Y. Liu, H. Qiu, H.M. Li, et al., Ind. Crop. Prod. 216 (2024) 118792.
[24] J.Y. Xie, Z.X. Wang, W.Y. Liu, et al., J. Nat. Prod. 86 (2023) 1910–1918.
[25] J.Y. Xie, Q.H. Jin, J.M. Gao, et al., Nat. Prod. Res. 36 (2020) 3520–3528.
[26] J.Y. Xie, P.F. Li, X.T. Yan, et al., Commun. Chem. 7 (2024) 1.
[27] X.T. Yan, J.X. Chen, Z.X. Wang, et al., J. Nat. Prod. 86 (2023) 119–130.
[28] J.F. Zong, Z. Hu, Y.Y. Shao, et al., Org. Lett. 22 (2020) 2797–2800.
[29] J. Nathan, A. Ramachandran, et al., J. Biochem. Mol. Toxicol. 36 (2022) e22954.
[30] W.C. Lee, S. Kopetz, I.I. Wistuba, et al., Ann. Oncol. 28 (2017) 2045–2047.
[31] M. Castaneda, P.D. Hollander, N.A. Kuburich, et al., Semin. Cancer Biol. 87 (2022) 17–31.
[32] M.A. Jordan, L. Wilson, Nat. Rev. Cancer 4 (2004) 253–265.